Linking Central Valley Deep Aquifer Recharge and High Sierra Nevada Snowpack

S. Werth[1], M. Shirzaei[1], G. Carlson[1], and Roland Bürgmann[2]

[1]Department of Geosciences, Virginia Polytechnic Institute and State University, Blacksburg, VA, USA.

[2]Dept of Earth and Planetary Science, University of California, Berkeley, CA, USA.

Corresponding author: Susanna Werth (swerth@vt.edu)

Key Points:

- High Sierra snowpack link to deep Central Valley aquifers via mountain block recharge is consistent with satellite & in-situ observations.
- Peak groundwater levels lag Sierra's water peak by one month, consistent with fluid diffusion time in Sierra's fractured crystalline body
- New hydroclimate models should account for the role of the Sierra Nevada in California's water cycle

Abstract

California's arid Central Valley relies on groundwater pumped from deep aquifers and surface water transported from the Sierra Nevada to produce a quarter of the United States' food demand. The natural recharge to deep aquifers is thought to be regulated by the adjacent high Sierra Nevada mountains, but the underlying mechanisms remain elusive. We investigate large sets of geodetic remote sensing, hydrologic, and climate data and employ process-based models at annual time scales to investigate possible recharge mechanism. Peak annual groundwater storage in the Central Valley lags several months behind that of groundwater levels, which suggests a longer transmission time for water flow than pressure propagation. We further find that peak groundwater levels lag the Sierra Nevada snowmelt by about one month, consistent with an ideal fluid pressure diffusion time in the Sierra's fractured crystalline body. This suggests that Sierra Nevada snowpack changes likely impact freshwater availability in the Central Valley aquifers. Our datasets, analysis and process-based models link the current precipitation and meltwater in the high mountain Sierra to deep Central Valley aquifers through the mountain block recharge process. We call for new hydroclimate models to account for the role of the Sierra in California's water cycle and for revision of the current management and drought resiliency plans.

Plain Language Summary

Current trends in hydrology and climate indicate a future in which extreme droughts will likely become the norm for drier regions. To sustain food production in the Central Valley, California, a major agricultural producer in the United States with a semiarid climate, groundwater supply and recharge are crucial to management solutions. We report the first remote-sensing observations directly linking Sierra Nevada's snowpack and groundwater storage to Central Valley's deep aquifer system recharge. We highlight the importance of high mountain groundwater systems in the water cycle, significantly contributing to recharging valley aquifers. We suggest that Sierra Nevada snowmelt and mountain recharge processes should be included in Central Valley aquifer models for accurate forecasting of the impact of climate extremes on groundwater supply and for developing effective drought adaptation and resiliency plans.

1 Introduction

Understanding key natural and artificial processes in recharging aquifer systems is essential for sustainable water management to store water for future use (Escriva-Bou et al., 2020, 2021; Ghasemizade et al., 2019). In arid and semiarid regions, such as the lowland Central Valley (CV) of California adjacent to the Sierra Nevada Mountains (Fig. 1a), artificial (or intentional) recharge through basins, unlined canals, and injection contributes to the net recharge, however, due to the natural disconnect between groundwater overdraft in dry areas and surface water surplus in wet areas, these contributions are likely small (Alley, 2002; Ayres et al., 2021; Escriva-Bou et al., 2021; Siebert et al., 2010; Zektser & Everett, 2004). Thus, large-scale natural recharge to deep aquifers is essential for replenishing dryland groundwater resources. In contrast to artificial recharge, the mechanism of natural recharge to deep aquifers remains elusive in the CV.

California's wet and dry seasons occur during November-April and May-October, respectively, with a large portion of the Sierra Nevada's precipitation falling as snow during the winter that supplies snow melt in spring (Fig. S1, S2). The Sierra Nevada's snowpack is thought to regulate surface water availability in the CV during the summer (Faunt, 2009; Peterson et al., 2003; Urióstegui et al., 2017). Isotope studies and streamflow analysis of snow-dominated mountainous watersheds of the western USA suggest that snowpacks via snowmelt significantly contribute to groundwater recharge, depending on present geology (Earman et al., 2006; Tague et al., 2008; Tague & Grant, 2009). But the mechanism linking the Central Valley's deep aquifer recharge to precipitation, underground storage, and water transport in the Sierra Nevada Mountains is not well-understood (Huth et al., 2004; Jódar et al., 2017; Liu et al., 2017).

Deep valley aquifers adjacent to high mountains, such as the CV, are thought to be recharged by lateral flows from higher elevations (Feth, 1964). The two main processes considered are Mountain Front Recharge (MFR) and Mountain Block Recharge (MBR, Fig. 2) (Somers & McKenzie, 2020). MFR often directly recharges shallow unconfined aquifers and causes a rise in the water table near streambeds from the mountain front to the basin aquifer. MBR replenishes deeper, often confined, and semi-confined aquifers laterally connected to high mountain aquifers (Somers & McKenzie, 2020). MBR occurs through fractures in the mountain block hydraulically connected to deep valley aquifers. Despite their proximity, there is no consensus on the role of especially MBR from the Sierra Nevada's granitic bedrock block into the CV aquifers; thus, it is not considered in current large-scale hydrological models used in water management assessments (Faunt, 2009; Hanson et al., 2012; Markovich et al., 2019). Meixner et al. (2016) lumped both processes to mountain system recharge (MSR) and estimated that it accounts for ~20% of GW recharge in the CV. Recent modeling experiments indicate that MFR drives almost all of the MSR to the CV aquifers (Schreiner-McGraw & Ajami, 2022). However, another study based on hydrological modeling concludes that MBR is more important and contributes up to 23% of the total GW recharge to the CV (Gilbert & Maxwell, 2017). These hydrogeological studies generally agree on the role of MSR components. However, they disagree on the importance of MBR for recharging deep valley aquifers of the CV, while the spatial extent of their investigations remains at scales of smaller watersheds that do not cover the entire CV.

An observation of groundwater volume change at the scale of the CV is available from remote sensing techniques, e.g., via their impact on the gravity field observed by the Gravity Recovery And Climate Experiment (GRACE) or on surface deformation observations with Global Navigation Satellite System (GNSS) or Interferometric Synthetic Aperture Radar (InSAR). Some studies, e.g., Murray & Lohmann (2018), Neely et al. (2021) analyzing high-resolution deformation maps, suggest direct recharge of deep aquifers from the surface of the CV following heavy precipitation events and surface water supply surplus during wet years, ignoring the impermeable clay layers separating shallow and deep aquifers (Faunt, 2009; Shirzaei et al., 2019) and that there is no evidence of vertical fractures (Carlson, Shirzaei, Ojha, et al., 2020) in the Valley to provide a direct pathway for the downward flow of surface water. Argus et al. (2022) use remote sensing data and hydrological models to quantify MBR from the Sierra Nevada to the CV at about 5 km^3/yr, though they fail to provide a feasible conceptual or physical model describing the deep aquifer recharge mechanisms.

Quantifying the spatiotemporal relationship between California's high mountains and deep valley aquifers is essential for developing appropriate plans supporting sustainable groundwater use. In the climate change era, when drought frequency and intensity have

increased globally (Fox-Kemper et al., 2021), including in California (Fig. S3), elevation-dependent warming (Pepin et al., 2015) disproportionally impacts the water availability and storage in high mountains. During the last decades specifically, increased evapotranspiration, decreased or delayed precipitation, and snowfall have caused severe snow droughts in the western USA, including the Sierra Nevada (Harpold et al., 2017; Hatchett & McEvoy, 2018; Mote et al., 2018). These droughts also reduce supply for the MBR. Hence, ignoring the MBR contribution may cause an overestimation of the lowland aquifer resilience to climate change and excess freshwater demand.

During a dry year, up to 70% of the groundwater used in CV is pumped within the growing season, mainly between April to June (Faunt, 2009), causing a long-term decline in groundwater levels, with the fastest rates observed in the southern San Joaquin basin (Fig. 1a, including the Tulare basin) (Faunt, 2009; Faunt et al., 2016; Konikow, 2015; Massoud et al., 2018; Ojha et al., 2018). Given the poor quality of shallow water in the southern CV (Hanak et al., 2017), most groundwater demand is addressed by tapping into deep aquifers at ~50 m to ~500 m depth below the surface, overlain by the confining layer of the Corcoran Clay or other clay lenses (Fig. 1a). Thus, direct percolation of surface water into deep aquifers is implausible (Shirzaei et al., 2019), at least at the time scale of a month to a year, corroborated by groundwater-age data (McMahon et al., 2011). For instance, Burow et al., (2007) reported a recharge rate of less than 600 mm/yr for unconfined aquifers in San Joaquin Valley. Thus, ancient groundwater supports California's water supply today (Healy & Scanlon, 2010).

Here, we investigate several big time-dependent datasets, including groundwater level (GWL, Fig. 1a, S4), surface deformation from Interferometric Synthetic Aperture Radar (InSAR) and Global Navigation Satellite System (GNSS) (Fig. 1b, S5), Gravity Recovery and Climate Experiment (GRACE) satellite-derived total water storage (TWS), as well as soil storage (SoS), snow storage (SnS) and reservoir storage (ReS, Fig. 1c) from hydrological data sources. We further apply sophisticated time-frequency and correlation analysis to identify hidden and non-stationary patterns in time series, quantifying their relationships. We specifically focus on investigating seasonal (i.e., annual) variations in hydrologic and geodetic observation time series that are sensitive to groundwater dynamics and their inter-annual differences. Based on the analysis, we build a conceptual model for CV deep aquifer recharge that supports the importance of MBR and agrees with geodetic remote sensing data over the CV.

2 Materials and Methods

Our study leverages various hydrologic and geodetic datasets, signal processing, statistical methods and physical models to quantify groundwater dynamics in the CV and Sierra Nevada Mountains (Fig. 1a).

2.1. Water Storage Components, Precipitation, and Snow Melt

GRACE and GRACE Follow-on missions (hereafter referred to as simply GRACE) monitor monthly changes in the Earth's gravity field at a spatial resolution of ~300-400 km, which are converted to equivalent total water storage (TWS) changes close to the surface (Schmidt et al., 2008; Tapley et al., 2004). In California, associated mass variations can be attributed to the terrestrial water cycle dynamics at sub-seasonal to interdecadal time scales. Water flow and storage processes on and below the surface change the region's total amount of

148 water stored in the soil, snowcap, surface- (including reservoirs and rivers), and groundwater.
149 With that, GRACE total water storage variations reflect water loss, e.g., due to drought or human
150 activities like intense groundwater pumping, as a mass deficit. Vice versa, for wetter periods, the
151 surplus of water is detected. This allows for predicting groundwater storage in large aquifers if
152 storage changes in all other components can be quantified and removed from GRACE TWS
153 (Famiglietti et al., 2011; Scanlon et al., 2012).

154 Here, we derive groundwater storage (GWS) changes from GRACE observations using
155 an approach similar to Ojha et al. (2019). We retrieve GRACE TWS variations from the RL06
156 Level-3 product from NASA's Jet Propulsion Laboratory (JPL) that solves regional mass
157 variations at a resolution of 3-degree. We do not apply JPL-mascon scale factors, as we calculate
158 groundwater changes at this native resolution, and we assume leakage between the mascon tiles
159 to be neglectable. To separate GWS changes from GRACE TWS, we retrieve mass variations in
160 other storage compartments from multiple data sets. We acquire soil moisture variations from all
161 available soil layers in the NOAH, CLSM and VIC models of the Global Land Data Assimilation
162 System (GLDAS) Version 2.1 (Beaudoing & Rodell, 2016; Rodell et al., 2004) at 0.25 (Noah)
163 and 1-degree (CLSM and VIC) resolution, respectively, for the entire GRACE period. We
164 average the three models to one ensemble dataset for further analyses after resampling them to a
165 uniform 0.5-degree resolution (Fig. 1c). For comparison, we also retrieve soil storage changes
166 from the WaterGAP Global Hydrological Model (WGHM, version 2.2d) at 0.5-degree
167 resolution, which is available until 2016 (Fig. S12a). We integrate reservoir storage (ReS)
168 changes from 18 reservoirs with capacities larger than or equal to 0.9 km^3, inside the margins of
169 the two mascon cells covering the CV (GRACE region, Fig. 1b), which are retrieved from the
170 California Department of Water Resources (CDWR, 2017). Snow storage (SoS) changes are
171 acquired in the form of snow water equivalent from the Snow Data Assimilation System
172 (SNODAS) (NOHRSC, 2004) over the contiguous United States since the end of 2003. Monthly
173 water mass variations for each storage compartment are summed across the GRACE region and
174 the regionally aggregated SoS, SnS and ReS variations are removed from GRACE TWS
175 variations for this area, after Ojha et al. (2019). The resulting time series for each storage
176 compartment, including groundwater storage changes during both GRACE mission periods, are
177 shown in Figure 1c. We assume the GRACE based estimate of GWS to be dominated by
178 groundwater variations in the CV, where porosity of the aquifers is much larger than that in the
179 SN Mountains.

180 From the SNODAS dataset we further retrieve driving and output variables related to
181 snow cover, including 'solid'- and 'liquid precipitation', and 'snowmelt runoff at the base of the
182 snowpack', to investigate these fluxes in the Sierra Nevada Mountains (Fig. S1, S2) and their
183 correlation to groundwater dynamics.

184 2.2. Groundwater Levels

185 Groundwater availability in the CV is conventionally monitored as water level change in
186 observation and irrigation wells. The data archives from the United States Geological Survey
187 (USGS) and the California Department for Water Resources (CDWR) provide more than 40,000
188 records from wells within the CV. The records have varying start dates, not all are continuously
189 monitored until today, and only some records provide sufficient temporal sampling rates to study
190 seasonal variations in GWLs. For this study we have screened 'daily data' and 'field data'
191 archives from the USGS (USGS, 2021) as well as 'continuous data' and 'periodic data' archives

from CDWR (CDWR, 2019) in California and selected records that cover the GRACE mission period from 2002 to 2020. We have excluded records labeled as 'irrigation well' and only selected sites labeled 'observation well'. Water levels in irrigation wells are potentially affected by the localized reduction in pressure during and after pumping from the well. Levels in observation wells are more likely to represent a regional state of pressure and storage changes in the entire aquifer. In addition, we categorized data entries that are larger than 3.5 times the standard deviation of the detrended time series as outliers and excluded them. Moreover, about half of the records have daily sampling rates and we excluded entire records from the field/periodic datasets that have less than six entries per year on average. From the initial dataset, 2128 time series (371 from USGS and 1727 from CDWR) provide observation records during 2002-2020 inside the CV. Only 682 records cover at least three years with less than 3 months of gap (Fig. S4); of those, we select 457 records gathered at depths deeper than 50 m since we want to focus on time series measured in semi-confined and confined aquifers. About half of the 457 available records are longer than 10 years (Fig. S4a-c). We note that these records were taken at only 250 unique well locations (circles in Fig. 1a), with some sites containing up to five nested level meters (Fig. S4d). Most deep sensors at each site are located 50 m to 300 m below the surface, with about half of the sensors reaching not more than 200 m deep and only a few are 450 m deep or deeper (Fig. 1a, S4e, f). Most usable wells are in the northern Sacramento Valley and only two dozen sites are in the southern San Joaquin Valley, where only 22 wells measure water level variations at depths below the Corcoran clay. Examples of GWL time series are shown in Figure 1a.

2.3. Surface deformation

Surface deformation due to TWS change, including GWS, occurs through two different processes. Total water mass deforms Earth's elastic crust, resulting in subsidence for an increase and uplift for a decrease in water mass. This deformation process has been described and inverted to quantify TWS in California (Adusumilli et al., 2019; Argus et al., 2022; Borsa et al., 2014; Carlson et al., 2022; Carlson, Shirzaei, Werth, et al., 2020; White et al., 2022). A second poroelastic deformation process is due to only groundwater changes occurring in semi-confined or confined aquifers, where pore spaces and granular matrix of rocks compact and groundwater levels fall under reduced water pressure. The opposite happens for increasing water pressure. Changes in water pressure in an aquifer can either be caused by net recharge or discharge, i.e. GWS change, in the aquifer itself, or initiated by water pressure propagating between the aquifer and a hydraulically connected outside region (Fetter & Kreamer, 2022). Decades of falling groundwater levels in the CV deep aquifers have caused continuous land subsidence at the surface and have been observed to be most severe during droughts (Galloway et al., 1999; Ojha et al., 2018; Smith et al., 2017; Vasco et al., 2022). It has been shown that elastic loading deformation in California is of the opposite sign and up to two magnitudes smaller than the poroelastic deformation occurring at the surface of the CV (Carlson, Shirzaei, Werth, et al., 2020).

To study seasonal variations in vertical land motion (VLM) since the early 2000s, we use vertical deformation time series from the daily tenv3 GNSS solutions from the Nevada Geodetic Laboratory (NGL). The solutions are processed at NGL using GipsyX software and are transformed into the IGS14 reference frame. Additional processing information can be found on the NGL website (http://geodesy.unr.edu/gps/ngl.acn.txt). We do not apply any further corrections to the GNSS time series for the rest of the analysis. From 1184 stations in California,

we selected 170 with a minimum record of 5 years between 2002-2020 and exhibiting a seasonal amplitude larger than the time series median standard deviation. Most stations began observations around 2008, with a length of 15 years (Fig. S5b). Of these stations, 37 are located within the CV boundaries (red triangles, Fig. 1b). Example time series at three sites throughout the study area are shown in the inset of Figure 1b. We determine the seasonal component of GNSS vertical land motion and the timing of maximum uplift and maximum subsidence using a time-frequency analysis (see Section 2.4).

We further measure the surface deformation in terms of line-of-sight (LOS) over the southern CV using Interferometric Synthetic Aperture Radar (InSAR). The SAR dataset includes 238 C-band images from descending track, path 144, of Sentinel-1A/B satellites spanning 2015/11/27-2022/12/20. We apply multi-looking factors of 32 and 6 in range and azimuth to obtain a pixel dimension of ~75m by ~75m. We use GAMMA software (Werner et al., 2000) to create a large set of interferograms. The interferograms are selected, so they form triplets, and the numbers of short, medium, and long temporal baseline pairs are comparable to minimize the phase closure error impact (Lee & Shirzaei, 2023). We apply the wavelet-based InSAR (WabInSAR) (Lee & Shirzaei, 2023; Shirzaei, 2013; Shirzaei et al., 2017) algorithm to perform a multitemporal interferometric analysis of the SAR dataset and create high-accuracy maps of surface deformation time series. A Shuttle Radar Topography Mission (SRTM) Digital Elevation Model (DEM) of 1-arcsecond (~30 m) spatial resolution (Farr et al., 2007) and precise satellite orbital information are used to estimate and remove the effect of topographic phase and flat earth correction (Franceschetti & Lanari, 1999). The absolute phase values are obtained by applying a 2D minimum cost flow algorithm (Costantini, 1998), then combined to create a Line-of-Sight (LOS) time series of surface deformation by using a reweighted least squares approach. The spatially correlated and temporally uncorrelated atmospheric delay are also estimated and removed (Shirzaei, 2013).

2. 4. Time-Frequency Analysis

To investigate the temporal variations in water storage components, GWLs, and deformation data, we perform a time-frequency analysis using a continuous wavelet transform, following Shirzaei et al. (2013). The wavelet transform allows decomposing signals into building blocks based on frequency contents. In contrast to the Fourier transforms, the wavelets can handle non-stationary signals and localize the signal energy in the time and frequency domain (Goswami & Chan, 1999). Wavelets have a key parameter scale (or dilation), which stretches or squishes the wavelet function and relates to the analyzed signal frequency. To perform wavelet analysis, we use the Matlab packages provided by Torrence and Compo (1998) and Erickson (2019) and apply the wavelet family of derivatives of gaussian (DOG, Fig. S6) at 200 levels of decomposition or scales. The temporal sampling of all time series is either daily or resampled at daily intervals.

Figures 3 and S7 illustrate our approach with an example of groundwater level time series at the DWR well 387793N1218123W004 (Fig. S7a). The wavelet power spectrum map (PSM, Fig. 3a and S7b) shows the signal's energy breakdown into several frequency components and their relative importance based on the amplitude of the PSM. A cone-of-influence overprinted on the spectrum indicates areas where edge effects play a role, and therefore, the PSM cannot be interpreted. Signal energy in areas inside the cone of influence is strongest at periods of about one year, with contour lines indicating their statistical significance with respect to white and red noise (with a lag-1 autocorrelation parameter of 0.85 for the latter) (Torrence & Compo, 1998).

Figure 3 also shows examples of wavelet PSM for selected GWL, VLM, and TWS component time series.

To isolate the annual component from the time series, we set the PSM to zero except for periods between 0.75-1.25 years and then apply an inverse wavelet transform of the new PSM (Fig. S7c). This approach considers that the annual components in climate-related processes do not have an exact one-year period. We further analyze the reconstructed annual signals to characterize the timing of annual maxima, minima, and the timing of fastest rate declines and increases (blue, red, and gray circles in Fig. S7c). We summarize the annual values for several years through temporal averaging using the median operator to retrieve the timing of maximum in the annual signal (e.g., as shown in Fig. 4). The same approach is applied to the time series of GWL, TWS components, GNSS and InSAR vertical deformation.

Probability density functions (PDFs) for spatiotemporal variation of timing of annual peaks were calculated using MATLAB's probability density estimator *kdensity()*,based on a normal kernel function for univariate distributions and applies a kernel smoothing window with an optimized bandwidth for normal densities.

2.5. Vertical Diffusion Model

In the high Sierra Nevada Mountains, a significant portion of snow melt water (Fig. S1, S2) infiltrates into the ground and recharges top aquifer layers (Peterson et al., 2003; Urióstegui et al., 2017), which are hydraulically connected to the CV aquifer system (Faunt, 2009). Here, to obtain the first-order approximation of the diffusion time, namely the time it takes for snow melt-related pore-fluid pressure increase in the Sierra to reach deep aquifer layers of the CV via MBR, we apply a first-order process-based 1D diffusion model following (Saar & Manga, 2003). The vertical propagation of hydrostatic pore-fluid pressure P' at depth z over time t is governed by the diffusion equation:

$$\kappa \frac{\partial^2 P\prime}{\partial z^2} = \frac{dP\prime}{dt}\,. \tag{1}$$

with the hydraulic diffusivity $\kappa = K/S_s$, which controls how fast pressure will propagate to depth. It is given by the ratio of vertical hydraulic conductivity K to specific storage S_s. The diffusivity of unfractured granite bedrock has values of around $\kappa = 10^{-4}\ m^2/s$ (Wang, 2000). However, for fractured volcanic rock, values as high at 0.3 m^2/s (Saar & Manga, 2003), and 1 m^2/s (Gao et al., 2000), consistent with the range provided by Talwani and Acree (1985), or even up to 7.9 m^2/s (Montgomery-Brown et al., 2019) are suggested. Here, we consider diffusivity values of 0.1, 0.3 and 0.5 m^2/s for Sierra's crystalline fractured rocks.

We solve the parabolic differential Equation 1 using the function *pdepe*() from the Matlab software by setting the initial pressure conditions to zero and the boundary conditions of the pore-fluid pressure to a periodic variation with periodicity ψ of 1 year, annual amplitude P_{max} and annual phase φ_0:

$$P'_{z,t=0} = P_{max} \cdot \cos\left(\frac{2\pi}{\psi} t + \varphi_0\right), \tag{2}$$

where at depth z, pore-fluid pressure is $P_{z,t} = P_{z,t-1} + P'_{z,t}$. We are only interested in changes $P'_{z,t}$ of pore-fluid pressure.

Assuming saturated conditions and solving Equations 1 and 2 for t allows us to estimate the time it takes to increase pore-fluid pressure annually due to groundwater recharge reaching vertically from top groundwater layers to depth z. The duration of pressure propagation to deep aquifer layers is independent of the amplitude of pressure change at the surface and a normalized solution for $P'_{z,t=0}/P_{max}$ is sufficient. The time delay estimate is most sensitive to the magnitude of the hydraulic diffusivity κ (Eq. 1) as well as the phase φ_0, of the annual pressure variation due to recharge (Eq. 2). We assume that the horizontal diffusivity of the aquifer is large enough, so the lateral diffusion time is relatively negligible (Fetter & Kreamer, 2022).

The annual phase of pressure variations in upper groundwater layers in the high Sierra Nevada Mountains φ_0 may be derived from the annual variation in water available for recharge in this region, which we quantify as follows. The top groundwater layers in the Sierra Nevada receive inflow from snow melt water and liquid precipitation (i.e., rainfall). Urióstegui et al. (2017) and Bales et al. (2011) found that only 10-20% of the snow melt water in the Sierras runs off through streams, with the remainder being lost to drainage into deep layers and evapotranspiration. We assume that all of the melt water initially increases pressure in the upper groundwater layers of the Sierra Nevada Mountains, before evaporating or running off. Also, we neglect the delay between the time that water for infiltration becomes available and its percolation into the upper groundwater layers of the Sierra Nevada Mountains. We consider these assumptions reasonable for wide areas of exposed fractured bedrock and given that we are only interested in quantifying the phase, not the absolute value of maximum pressure variations. For that, we retrieve the time series of SNODAS dataset variables 'snowmelt runoff at the base of the snowpack' M and 'liquid precipitation' P_{liqu} (see Section 2.1, Fig. S1) averaged for the drainage area of the Sierra Nevada toward the CV (rose-shaded area in Fig. 1a). We correct liquid precipitation for canopy interception by a relative value of 20% (Vrugt et al., 2003), as this intercept changes the relative amplitudes between M and P_{liqu}, and therefore, it can impact the annual phase. Finally, we get a time series of total water available for recharge in the Sierra Nevada drainage area from $(P_{liqu} - 0.2 \cdot P_{liqu} + M)$ and quantify monthly mean values of this time series during 2002-2020 (Fig. S2c). We also determine the mean timing of the annual peak for each year and at each location in the drainage area, which we apply as the timing of the annual maximum of the pressure variation to constrain φ_0 for the boundary condition in Equation (2).

4 Results

4.1. Year-to-Year Water Variability

The time series of TWS variations obtained from the GRACE satellites (Tapley et al., 2004, 2019) and their components measured through in-situ observations (e.g., wells) (Alam et al., 2021) or water balance models (Faunt, 2009; Li et al., 2018) are characterized by annual variations attributed to overall dynamics in the terrestrial water cycle (Tang & Oki, 2016). Several example time series are shown in Figure 1c. A less obvious pattern comprises the interannual variations in the amplitude of the annual signal. Identifying the amplitude and timing of the peak annual and interannual signal components allows for resolving the temporal scale at which the connected systems interact.

To this end, we apply the wavelet-based time-frequency analysis to extract hidden patterns in the datasets (see Section 2.2.1, Fig. S6). The results from the time-frequency analysis

are shown in the form of a PSM, distributing the signal's power into frequencies (or periods) and time intervals (Fig. 3, S7). We find maximum amplitudes characterize the PSMs associated with different time series at equivalent periods of 1 year and 3-8 years (Fig. 3). These frequency components are associated with general variations in water availability associated with atmosphere-ocean interactions, influencing water cycles in the Southwest USA (Quiring & Goodrich, 2008). Significant drought periods, such as during 2007-2009 and 2012-2015 (Fig. S3), correspond with cool phases of El Niño Southern Oscillation (ENSO) recurring every 3-7 years, the cool phase of the Pacific Decadal Oscillation (PDO), and the warm phase of the Atlantic Multidecadal Oscillation (AMO) (McCabe et al., 2004; Quiring & Goodrich, 2008). The length of our observation does not allow for resolving signal components over a decade or longer, as indicated by the cone of influence, the shaded region in the PSM.

Some PSMs also show unique patterns. For instance, the PSMs of GWL changes (Fig. 3a) and GNSS VLM (Fig. 3b) exhibit components at periods of 0.5 and 3 years, albeit the component of 0.5 years for VLM disappears following 2008. In contrast, the PSM of SnS (Fig. 3e) shows only a transient component over a period of 3 years. PSM of GWS variations (Fig. 3g) shows a transient component of 1 year period. Notably, the location and amplitude of peak PSM are not constant and change over time, especially for TWS, SnS, ReS, and GWS variations and to a lesser extent in SoS due to water availability changes within wet and dry seasons and in between them as well as due to human interventions. For instance, the amplitude of annual components was reduced or diminished during the drought years 2007-2010 and 2012-2015. During these periods, reservoirs were not refilled, and the Sierra Nevada received little precipitation, reducing the amplitude of the corresponding annual components (Fig. 3e and 3f). The amplitude of the annual component of GWS variations vanishes during the same years (Fig. 3g).

Figure 3h presents the isolated annual components for all the time series comprising PSM components of 0.75 to 1.25 yr periods, which display non-stationary behaviors, i.e., the amplitude changes over time. We find that year-to-year TWS is experiencing the most pronounced changes and GWS the least. We also note that year-to-year peak extremes do not co-occur for different time series. For instance, during the 2012-2015 drought, TWS, SoS, and ReS variations experienced their lowest amplitudes in 2013 and 2014, while that of GWS occurred two years later during 2016, following the snow-poor years in 2014 and 2015. Characterizing such inter-annual variability in water cycle components improves understanding of hydroclimate extremes and water storage capacity in the region (Yin & Roderick, 2020).

4.2. Timing of the Seasonal Signal

We further investigate the spatial variability of the timing of the peak annual amplitude of TWS and its components across the study region (Fig. 4). Note that spatial detail cannot be resolved from the GRACE TWS with 300-400 km spatial resolution. To this end, we find the day-of-year (DOY) corresponding with the peak of the timeseries of the annual components and then obtain the median of DOY for each time series. Figure 4 plots the median peak DOY for each dataset at their original spatial resolution, except for GWL and VLM, where the values are interpolated with an inverse distance weighting scheme and a 25 km radius. The median peak DOY for GWL is uniform across the Valley (Fig. 4a, S8) with negligible interannual variability (Fig. S9). GWL peaks occur from February to March (Fig. 4a, S8a) and minima in August (Fig.

S8b). The fastest GWL rate increase (i.e., the mid-point between annual minima and maxima) occurs during November (Fig. S8c), and the fastest GWL rate decrease (i.e., the mid-point between annual maxima and minima) occurs during May (Fig. S8d). These observations are consistent with the timing of maximum pumping in the CV during April-June. A linear correlation of 0.3 was found between observation well depth and peak DOY, indicating GWL rises slightly later in the year at deeper wells (Fig. S8a, left inset). Compared with GWL, the median peak DOY of GNSS VLM in the CV is spatially more variable (Fig. 4b and S10), with negligible interannual variability (Fig. S11). We find a bimodal distribution for this peak DOY (inset in Fig. S10a), with about a third of the stations within the CV peaking from March to April and most of the remaining stations from September to October. A bimodal behavior is also observed in the median DOY of annual VLM minima. The median DOY of the fastest VLM rate increases and decreases are also obtained (Fig. S10), indicating a smaller interannual variability than that of peak DOY (Fig. S11). We further estimate the median peak DOY of TWS, SoS, SnS, ReS, and GWS within the GRACE region (Fig. 1b), all of which show spatially uniform patterns but are distinct from each other (Fig. 4c-g), with spatial DOY averages of 93, 70, 65,102, and 156 days, respectively.

We performed a similar analysis using InSAR LOS deformation observations. Figure 5a shows the LOS velocity field measuring up to 18.5 cm/yr subsidence in some parts of San Joaquin Valley. We obtained seasonal phase (peak DOY) and amplitude (Fig. 5b, c) for the southern CV covered by the Sentinel-1 frame. The spatial distribution of median peak DOY generally agrees with that of GNSS (Fig. 4b). The denser spatial sampling from the InSAR analysis, however, reveals an outward propagation of the median annual peak DOY from the center of CV. Although it varies yearly, the overall outward propagating pattern of peak DOY remains similar through wet and dry years (Fig. S15). We note that this result is opposite to what was found by Neely et al. (2021), who suggested an inward propagation of the annual peak towards the center. Figures 5c and S16 show the median and yearly seasonal amplitude of surface LOS deformation, reaching up to 4 cm, with the largest value during dry years.

Next, we investigate the empirical probability density function (PDF) of annual peak DOY associated with all components of TWS and deformation and several other relevant hydrological datasets (Fig. 6). Shown are normalized PDFs of annual peak DOY obtained for each year and each time series without temporal averaging, thus the interannual variabilities are preserved. Comparing different PDFs, we find for the Sierra Nevada that precipitation generally peaks in early January, with a mean DOY of 16 (Fig. 6a), meltwater in late February, DOY 55 (Fig. 6c), and the total water availability (combination of precipitation, meltwater, and canopy interception) in late January, DOY 22 (Fig. 6b). We obtain a wide distribution for the influxes, and years with a later maximum melt typically have a larger peak, causing the right-skewed distribution of annual peak DOY of snowmelt (Fig. S2b). The annual SoS peak for the CV occurs in March, DOY 70 (Fig. 6d), ~2-3 months after precipitation peaks. SnS peaks in March, ReS and TWS ~1 month later in April, while GWS of the CV peaks in June (Fig. 6e-g). The VLM minima (i.e., subsidence) across California, outside of the CV, co-occur with TWS maxima around April, DOY 93 (Fig. 6i). In contrast, GNSS VLM inside the CV (Fig. 6j) peaks together with GWL (Fig. 6k) around March, DOY 65, and ~3 months before GWS based on GRACE and composite hydrology (Fig. 6g). Peak VLM inside the CV derived from high-resolution InSAR maps (Fig. 6k, dashed line) have a more complex distribution, with the first peak co-occuring with GNSS and well levels around beginning of March and a later peak ranging from beginning to end of April. We further observe a delay of 43 days between total

453 water available for recharge in the Sierra Nevada Drainage area (DOY 22, Fig. 6b) and GWL in
454 the CV (DOY 65, Fig. 6k).

455 To investigate whether the mean values of the PDFs in Figure 6 were significantly
456 different, we performed a two-sample mean difference hypothesis test using the t-distribution
457 (Meyer, 1970). We formulated the null hypothesis so that the mean values were the same and
458 tested the hypothesis at a significance level of 0.05. The test was rejected, hence, the mean
459 values are statistically the same for all pairs of PDFs in Figure 6, except between GNSS uplift
460 (CV) and GWL (CV), between TWS and GNSS Subsidence (CA), between SnS (Sierra Nevada)
461 and GNSS uplift (CV), and between SnS (Sierra Nevada) and GWL (CV).

462 When estimating PDFs for the timing of annual peaks of SoS and GWS (Fig. 6e and 6g),
463 the variability among the individual SoS models was considered (Fig. S12). SoS timing varies by
464 about ~2 months from January to February (Fig. S12c). We propagate the variation of SoS
465 timing toward that of GWS by estimating GWS for each individual soil model (Fig. S13a). The
466 resulting annual GWS timing varies ~2 months from May to July (Fig. S13b,c). This variability
467 was included when calculating mean, median, standard deviation, and PDFs of annual GWS
468 timing (Fig. 6g). Although GWS also depends on the timing of TWS, SnS and ReS, annual
469 amplitudes of SnS and ReS are only 10% of TWS (Fig. 1c). Therefore they will only marginally
470 impact the calculation of annual timing of GWS. We assume a minimal measurement uncertainty
471 for the timing of TWS.

472 ### 4.3. Pressure Diffusion From the High Mountains to Deep Valley Aquifers

473 Earlier studies (e.g., Gilbert and Maxwell (2017)) have suggested that a natural
474 connection should exist between deep CV and High Sierra Nevada mountain aquifers through
475 the fractured granite of the mountain block. We provide a first-order estimate for the diffusion
476 time, the time it takes for a pressure front to vertically diffuse from the top aquifer layers in the
477 Sierra Nevada Mountains down to elevations of the deep CV aquifers (Section 2.5, Eq. 1). If we
478 quantify that using a hydraulic diffusivity $\kappa = 0.3$ m^2/s for Sierra's crystalline fractured rocks, it
479 takes 18-36 days for the pressure to travel vertically to depth of 600-1300 m (Fig. 7). We further
480 consider a range for the vertical hydraulic conductivity and evaluate the diffusion time for $\kappa =$
481 0.1 m^2/s and $\kappa = 0.5$ m^2/s to depth of 600-1300 m, corresponding with 34-73 days and 12-23
482 days (Fig. S14), respectively.

483 ## 5 Discussions and Conclusions

484 This study performs time-frequency analyses of large hydrologic and geodetic datasets across
485 California with various spatiotemporal resolutions and uncertainties to characterize the annual
486 peak DOY, interannual peak amplitude variations, and correlative behaviors across these
487 observations. We observe relatively low seasonal peaks during droughts for all water storages
488 (Fig. 3h). However, only for storages in snow and groundwater wavelet PSMs vanish completely
489 at periods of around one year during droughts when snow cover was diminished to absent during
490 2007 and 2012-2015 (Fig. 1c, 3e, 3g). We interpret this correlation as an indicator that the
491 volume of the snowpack and the following snowmelt played a substantial role in groundwater
492 recharge in the CV. Once corrected for SoS, SnS, and ReS, GRACE measures a combination of
493 GWS change in shallow and deep aquifers. Hence, we consider snow to be relevant for both
494 MFR and MBR, with the former mechanism being more relevant for replenishing the shallow

and the latter more relevant for (slow) flow to the deep aquifers, given the depth of their flow path.

We further observe that GNSS VLM and InSAR LOS peak DOY vary across California. The peaks for stations inside the CV co-occur with that of GWL (Fig. 6j, k), specifically at the sites near the center of the Valley, where aquifer confining layers are thick and observed annual amplitudes are large (Fig. 5). This indicates the presence of poroelastic aquifer deformation due to groundwater pumping (Ojha et al., 2018; Smith et al., 2017). In contrast, the VLM peak minima for stations outside the Valley co-occur with that of TWS peak maxima (Fig. 6h, i), attributed to the variations in elastic water loading (Argus et al., 2017; Carlson et al., 2022; Johnson et al., 2017). Interannual variability in the peak amplitudes impacts the hydroclimate trends, changing baselines used to assess the future risk of climate extremes and vulnerability of water resources (Stevenson et al., 2022). In summary, a similar peak DOY suggests that some components of the hydrological system act in concert with or respond elastically to similar forcing of the hydroclimate or to anthropogenic factors. In contrast, a different peak DOY may indicate a cascading nature of the response to forcing governed by a time-dependent process.

Here we propose that MBR is the fundamental process, allowing long-term recharge to deep aquifers in the CV. The feasibility of this mechanism is demonstrated in Fig. 7, where a first-order process-based pressure diffusion model quantifies the lag between peak pore pressure in the Sierra Nevada aquifers due to snowmelt and peak pore pressure within deep CV aquifer layers. We estimate the lag at about a month, ignoring the lateral diffusion time, which is often negligible for permeable aquifers such as CV (Fetter & Kreamer, 2022). Given the uncertainty range of hydraulic diffusivity (Somers & McKenzie, 2020), the estimated diffusion time agrees well with the lag between peak water availability in the mountains and peak water level in deep aquifers (Fig. 6b and k). This agreement supports the hypothesis that high mountain aquifers are connected to deep valley aquifers through pressure propagation from MBR, and that it drives seasonal well level changes in the deep CV aquifers. The peak GWL in March likely occurs early due to anthropogenic influence since heavy groundwater pumping typically onsetting from April to May. A later GWL peak would suggest a longer vertical diffusion time, consistent with the considered range for tested hydraulic conductivities.

We further observed an outward migration of the InSAR LOS peak DOY from the center of CV (Figs. 5 and S15), which is at odds with the previously published works (e.g., Neely et al., 2021) that suggested an inward propagation of annual peak DOY from the Sierra Nevada Mountains toward the center of the CV. They suggested that MFR fed by surface water flowing off the Sierra Nevada may replenish aquifers (deep and shallow) seasonally across the southern CV (Neely et al., 2021). However, the MFR mechanism is implausible to recharge deep confined aquifers (Shirzaei et al., 2019) due to the presence of the impermeable Corcoran clay layer and other clay lenses (Faunt, 2009) and little evidence of widespread vertical cracks and deep extensional fissures in the Valley (Carlson, Shirzaei, Ojha, et al., 2020) to provide a potential pathway for water to percolate deep into the aquifers, though further research on tension cracking and fissure initiation in the Valley is needed (Carlson, Shirzaei, Ojha, et al., 2020). In contrast, our hypothesis of MBR linking Sierra groundwater to deep CV's aquifers is consistent with Darcy's fluid flow law, linking the fluid discharge rate to the hydraulic head gradient between two given points, scaled with the hydraulic conductivity. Under constant hydraulic conductivity, the largest discharge happens to the point of the lowest hydraulic head. In CV, it is logical to assume the zone of the fastest subsidence rate is where the heads are lowest, consistent

with groundwater level observation. Thus the recharge from Siera should replenish aquifers near the center of Valley first and then propagate outward from the center to areas with smaller hydraulic gradients, as observed here. Hence, we interpret the InSAR LOS observation of annual peak DOY as additional support for the hypothesis of a direct pressure link between the Sierra Nevada aquifers and CV deep aquifers through mountain block conduits.

An unexpected finding is the phase difference between annual peaks of GWL in deep confined aquifers, and GWS in the entire CV aquifer system (including confined and unconfined units, Fig. 4a, 4g, 6g and 6k) is about three months. This indicates that different processes influence GWS and well levels. In confined units, the well level change is driven by changes in groundwater storage and pore fluid pressure, while the gravity-derived measurements only detect the change in mass, hence, storage changes. During the spring, pressure rises faster in the deep aquifers than storage is recovered in the entire aquifer system. A vertical hydraulic connection via MBR flow paths would allow pressure change propagation from the mountain to CV aquifers at seasonal time scales. However, direct water seepage along MBR flow paths takes centuries to millennia (Berghuijs et al., 2022). The proposed mechanism here does not require water percolation and is consistent with the tracer findings that deep groundwater in the CV is primarily old (McMahon et al., 2011). Our results further emphasize that vertical pressure propagation occurs faster than net recharge (i.e., detected as storage change) from the mountain aquifers to the valley aquifers. The later peak in GWS might be primarily driven by annual variations in top unconfined aquifer layers (Vasco et al., 2022), which would recharge faster than deep aquifers. This is also consistent with the relatively late mean annual peak in melt water occuring during early May (see Fig. S2), hence, a long lasting supply for recharge through surface-groundwater links along the mountain fronts until late spring. At annual time scales, MFR likely contributes a significant portion to storage changes in shallow aquifers, and the seasonal variation in GRACE GWS mainly comprises such shallow aquifers instead of deep aquifers. In this case, the seasonal well level rises in deep CV aquifer layers may be driven dominantly by pressure variability rather than storage variability. It should also be noted that the MBR estimate based on GNSS/GRACE combination from Argus et al. (2022) was derived as the difference between gravity and elastic loading-based annual GWS estimates to the output of a hydrological model not including MSR. The authors interpret this difference solely as MBR and neglect the contribution of MFR in the estimate, owing that the method they apply cannot discriminate between the two MSR processes. To reliably quantify MBR at the scale of the CV and discriminate it from MFR, we suggest the implementation of a fully fluid-solid media coupled 3D groundwater model for the CV that integrates the wealth of hydrologic and remote sensing observations sensitive to dynamics in the aquifers as demonstrated in this study. The results should also be crosschecked with observations of groundwater ages, e.g. based on isotope studies (Earman et al., 2006).

Our findings are subject to uncertainties, albeit statistical tests of significance help corroborate the main results. The wavelet time-frequency analysis is affected by data gaps and variable sampling rates, similar to other spectral methods (Goswami & Chan, 1999), although the ability of the continuous wavelet transforms to localize signal components in time and space minimizes error propagation. GNSS sites may be affected by other processes causing annual oscillations, such as non-tidal loading, tectonic processes, thermoelastic deformation, and draconitic errors (Chanard et al., 2020). Errors in the GWS component from GRACE observations are subject to any error in the correction terms, which directly maps into the GWS time series. However, the three months delay between the peak of GWS and GWL remains

586 robust against the uncertainty in the timing of GWS (see Section 4.2). Hence, the measure that
587 pressure propagates faster to deep aquifer layers than the groundwater volume change in the
588 entire aquifer remains unaffected.

589 Recent studies (Ajami et al., 2011; Markovich et al., 2019; Meixner et al., 2016; Somers
590 & McKenzie, 2020; Wahi et al., 2008; Welch & Allen, 2014) have recognized mountains'
591 critical role in freshwater supply to lowland dry basins, debunking the outdated notion that
592 mountain groundwater storage and supply is negligible. In the Sierra Nevada aquifers,
593 cosmogenic isotope studies linking snowmelt and annual aquifer recharge indicate a strong link
594 between snowmelt and aquifer recharge and discharge in the mountains (Urióstegui et al., 2017).
595 Additional evidence is provided by the increased age of groundwater contributing to the spring
596 stream flow over the Sierra Nevada, consistent with increased temperature and reduced
597 precipitation at high elevations (Manning et al., 2012). Thus, the high Sierra Nevada snowpack is
598 essential for recharging mountain aquifers, which, in turn, contributes to the long-term recharge
599 of deep, confined CV aquifers. Sierra Nevada runoff and MFR's role in freshwater supply in the
600 CV is well-understood (Faunt, 2009; Meixner et al., 2016). However, the mountain block
601 recharge process proposed here to replenish deep aquifers is not considered in the current
602 hydrological models for the Valley, for example, by Faunt et al. (2009). Annual, interannual, and
603 long-term changes in snowpack directly impact the MFR and MBR from the Sierra Nevada
604 Mountains to the CV. Thus, the reliance on hydroclimate models that currently do not account
605 for MBR limits the ability to accurately forecast the risk of climate extremes to California's
606 groundwater supply and presents challenges for developing appropriate adaptation and resiliency
607 strategies. The observation and analysis presented here have implications for the CV's recharge
608 mechanism to deep aquifers. We call for new models that more comprehensively account for the
609 Sierra Nevada Mountains' role in California's water cycle, which may also require a revision of
610 current management and resiliency plans. Finally, we suggest the integration of pressure physics
611 into methods quantifying seasonal storage changes in CV aquifers that apply well data and
612 storage coefficients, or deformation data, given that well level and deformation changes at
613 seasonal time scales are also driven by a change in pressure, not only in storage.

614

615 **Acknowledgments**

616 We thank anonymous reviewers and the editor for constructive comments and
617 suggestions. This research was partly funded by the National Aeronautics and Space
618 Administration grants NNX17AD98G (SW, MS, GC), 80NSSC21K0419 (SW, MS, GC) and
619 80NSSC21K0061 (SW), as well as the Department of Energy grant DE-SC0019307 (MS).

620

621 **Open Research**

622 All data used for this study are publicly available from the following sources. GRACE data were
623 accessed from JPL PO.DAAC at https://podaac.jpl.nasa.gov/dataset/TELLUS_GRAC-
624 GRFO_MASCON_CRI_GRID_RL06_V2. SNODAS data were downloaded from the National
625 Snow & Ice Data Center (https://nsidc.org/data/g02158), GLDAS Noah, CLSM and VIC model
626 outputs from the Goddard Earth Sciences Data and Information Services Center via
627 https://disc.gsfc.nasa.gov/datasets/GLDAS_NOAH025_M_2.1/summary?keywords=GLDAS,

https://disc.gsfc.nasa.gov/datasets/GLDAS_CLSM10_M_2.1/summary?keywords=GLDAS, and https://disc.gsfc.nasa.gov/datasets/GLDAS_VIC10_M_2.1/summary?keywords=GLDAS, respectively. We kindly thank Hannes Müller Schmied (hannes.mueller.schmied@em.uni-frankfurt.de) at the University of Frankfurt for providing WGHM version 2.2d outputs. GNSS time series were downloaded from the Nevada Geodetic Laboratory (http://geodesy.unr.edu/gps_timeseries/tenv3/IGS14/). The California Department of Water Resources provided reservoir data (https://cdec.water.ca.gov/dynamicapp/getAll?sens_num=15) and groundwater level data, which we retrieved as bulk download from the California Natural Resources Agency via the California Open Data Portal for "Periodic Groundwater Level Measurements" (https://data.ca.gov/dataset/periodic-groundwater-level-measurements) and for "Continuous Groundwater Level Measurements" (https://data.ca.gov/dataset/continuous-groundwater-level-measurements). Further groundwater level data were retrieved from the USGS archives for "Daily Data" (https://waterdata.usgs.gov/ca/nwis/dv/?referred_module=gw) and "Field Measurements" (https://nwis.waterdata.usgs.gov/ca/nwis/gwlevels). Wavelet software packages are provided by C. Torrence and G. Compo at URL: http://atoc.colorado.edu/research/wavelets, as well as by Jon Erickson at URL: https://www.mathworks.com/matlabcentral/fileexchange/20821-continuous-wavelet-transform-and-inverse. InSAR results, assembled groundwater records as well as all data analysis results presented in the supporting information or figures will be made available upon acceptance through a repository with the Virginia Tech Data Repository (https://data.lib.vt.edu/). During peer review, all data analysis results are available in the supporting information, and/or figures.

References

Adusumilli, S., Borsa, A. A., Fish, M. A., McMillan, H. K., & Silverii, F. (2019). A decade of terrestrial water storage changes across the contiguous United States from GPS and GRACE. *Geophysical Research Letters*, 2019GL085370. https://doi.org/10.1029/2019GL085370

Ajami, H., Troch, P. A., Maddock, T., Meixner, T., & Eastoe, C. (2011). Quantifying mountain block recharge by means of catchment-scale storage-discharge relationships. *Water Resources Research*, *47*(4). https://doi.org/10.1029/2010WR009598

Alam, S., Gebremichael, M., Ban, Z., Scanlon, B. R., Senay, G., & Lettenmaier, D. P. (2021). Post-Drought Groundwater Storage Recovery in California's Central Valley. *Water Resources Research*, *57*(10). https://doi.org/10.1029/2021WR030352

Alley, W. M. (2002). Flow and Storage in Groundwater Systems. *Science*, *296*(5575), 1985–1990. https://doi.org/10.1126/science.1067123

Argus, D. F., Landerer, F. W., Wiese, D. N., Martens, H. R., Fu, Y., Famiglietti, J. S., Thomas, B. F., Farr, T. G., Moore, A. W., & Watkins, M. M. (2017). Sustained water loss in California's mountain ranges during severe drought from 2012 to 2015 inferred from GPS. *Journal of Geophysical Research: Solid Earth*, *122*(12), 10,510-559,585. https://doi.org/10.1002/2017JB014424

Argus, D. F., Martens, H. R., Borsa, A. A., Knappe, E., Wiese, D. N., Alam, S., Anderson, M., Khatiwada, A., Lau, N., Peidou, A., Swarr, M., White, A., Bos, M. S., Landerer, F. W., & Gardner, P. (2022). Subsurface water flux in California's Central Valley and its source watershed from space geodesy. *Geophysical Research Letters*. https://doi.org/10.1029/2022GL099583

Ayres, A., Hanak, E., Gray, B., Sencan, G., Bruno, E., Bou, A. E., & Collins, J. (2021). *Improving California' s Water Market*.

Bales, R. C., Hopmans, J. W., O'Geen, A. T., Meadows, M., Hartsough, P. C., Kirchner, P., Hunsaker, C. T., & Beaudette, D. (2011). Soil Moisture Response to Snowmelt and Rainfall in a Sierra Nevada Mixed-Conifer Forest. *Vadose Zone Journal*, *10*(3), 786–799. https://doi.org/10.2136/vzj2011.0001

Beaudoing, H., & Rodell, M. (2016). GLDAS Noah Land Surface Model L4 monthly 0.25 x 0.25 degree V2.1, NASA/GSFC/HSL: Greenbelt, Maryland, USA,. *Goddard Earth Sciences Data and Information Services Center (GES DISC)*. https://doi.org/10.5067/SXAVCZFAQLNO

Berghuijs, W. R., Luijendijk, E., Moeck, C., van der Velde, Y., & Allen, S. T. (2022). Global Recharge Data Set Indicates Strengthened Groundwater Connection to Surface Fluxes. *Geophysical Research Letters*, *49*(23). https://doi.org/10.1029/2022GL099010

Borsa, A. A., Agnew, D. C., & Cayan, D. R. (2014). Ongoing drought-induced uplift in the western United States. *Science*, *345*(6204), 1587–1590. https://doi.org/10.1126/science.1260279

Burow, K. R., Dubrovsky, N. M., & Shelton, J. L. (2007). Temporal trends in concentrations of DBCP and nitrate in groundwater in the eastern San Joaquin Valley, California, USA. *Hydrogeology Journal*, *15*(5), 991–1007. https://doi.org/10.1007/s10040-006-0148-7

Carlson, G., Shirzaei, M., Ojha, C., & Werth, S. (2020). Subsidence-Derived Volumetric Strain Models for Mapping Extensional Fissures and Constraining Rock Mechanical Properties in the San Joaquin Valley, California. *Journal of Geophysical Research: Solid Earth*. https://doi.org/10.1029/2020JB019980

Carlson, G., Shirzaei, M., Werth, S., Zhai, G., & Ojha, C. (2020). Seasonal and Long-Term Groundwater Unloading in the Central Valley Modifies Crustal Stress. *Journal of Geophysical Research: Solid Earth*, *125*(1), 1–17. https://doi.org/10.1029/2019JB018490

Carlson, G., Werth, S., & Shirzaei, M. (2022). Joint Inversion of GNSS and GRACE for Terrestrial Water Storage Change in California. *Journal of Geophysical Research: Solid Earth*, *127*(3). https://doi.org/10.1029/2021JB023135

CDWR. (2017). *California Department of Water Resources, California Data Exchange Center, Active Monthly Reservoirs*. http://cdec.water.ca.gov/misc/monthly_res.html

CDWR. (2019). *Continuous Groundwater Level Measurements*. http://wdl.water.ca.gov/waterdatalibrary/

Chanard, K., Métois, M., Rebischung, P., & Avouac, J. P. (2020). A warning against over-interpretation of seasonal signals measured by the Global Navigation Satellite System. *Nature Communications*, *11*(1), 1–4. https://doi.org/10.1038/s41467-020-15100-7

Costantini, M. (1998). A novel phase unwrapping method based on network programming. *IEEE Transactions on Geoscience and Remote Sensing*, *36*(3), 813–821. https://doi.org/10.1109/36.673674

Earman, S., Campbell, A. R., Phillips, F. M., & Newman, B. D. (2006). Isotopic exchange between snow and atmospheric water vapor: Estimation of the snowmelt component of groundwater recharge in the southwestern United States. *Journal of Geophysical Research Atmospheres*, *111*(9). https://doi.org/10.1029/2005JD006470

Erickson, J. (2019). *Continuous wavelet transform and inverse* (Retrieved August 30, 2019.). MATLAB Central File Exchange.

Escriva-Bou, A., Hui, R., Maples, S., Medellín-Azuara, J., Harter, T., & Lund, J. R. (2020). Planning for groundwater sustainability accounting for uncertainty and costs: An application to California's Central Valley. *Journal of Environmental Management*, *264*, 110426.

Escriva-Bou, A., Sencan, G., & Hanak, E. (2021). *Groundwater Recharge, Fact Sheet August 2021*.

Famiglietti, J. S., Lo, M., Ho, S. L., Bethune, J., Anderson, K. J., Syed, T. H., Swenson, S. C., de Linage, C. R., & Rodell, M. (2011). Satellites measure recent rates of groundwater depletion in California's Central Valley. *Geophysical Research Letters*, *38*(3). https://doi.org/10.1029/2010GL046442

Farr, T. G., Rosen, P. A., Caro, E., Crippen, R., Duren, R., Hensley, S., Kobrick, M., Paller, M., Rodriguez, E., Roth, L., Seal, D., Shaffer, S., Shimada, J., Umland, J., Werner, M., Oskin, M., Burbank, D., & Alsdorf, D. (2007). The Shuttle Radar Topography Mission. *Reviews of Geophysics*, *45*(2), RG2004. https://doi.org/10.1029/2005RG000183

Faunt, C. C. (2009). *Groundwater Availability of the Central Valley Aquifer, California* (C. C. Faunt, Ed.). U.S. Geological Survey Professional Paper 1766. https://pubs.usgs.gov/pp/1766/

Faunt, C. C., Sneed, M., Traum, J., & Brandt, J. T. (2016). Water availability and land subsidence in the Central Valley, California, USA. *Hydrogeology Journal*, *24*(3), 675–684. https://doi.org/10.1007/s10040-015-1339-x

Feth, J. H. (1964). Hidden Recharge. *Groundwater*, *2*(4), 14–17. https://doi.org/10.1111/j.1745-6584.1964.tb01780.x

Fetter, C. W., & Kreamer, D. (2022). *Applied Hydrogeology* (5th ed.). Waveland Press.

Fox-Kemper, B., Hewitt, H. T., Xiao, C., Aðalgeirsdóttir, G., Drijfhout, S. S., Edwards, T. L., Golledge, N. R., Hemer, M., Kopp, R. E., Krinner, G., Mix, A., Notz, D., Nowicki, S., Nurhati, I. S., Ruiz, L., Sallée, J.-B., Slangen, A. B. A., & Yu, Y. (2021). Ocean, Cryosphere and Sea Level Change. In *Climate Change 2021: The Physical Science Basis. Contribution of Working Group I to the Sixth Assessment Report of the Intergovernmental Panel on Climate Change [MassonDelmotte, V., P. Zhai, A. Pirani, S. L. Connors, C.*

Péan, S. Berger, N. Caud, Y. Chen,. Cambridge University Press, Cambridge, United Kingdom and New York, NY, USA, 2391 pp. doi:10.1017/9781009157896. https://report.ipcc.ch/ar6/wg1/IPCC_AR6_WGI_FullReport.pdf.

Franceschetti, G., & Lanari, R. (1999). *Synthetic aperture radar processing*. CRC Press.

Galloway, D. L., Jones, D. R., & Ingebritsen, S. E. (1999). *Land subsidence in the United States*. U.S. Geological Survey Circular 1182. https://doi.org/10.3133/cir1182

Gao, S. S., Silver, P. G., Linde, A. T., & Sacks, I. S. (2000). Annual modulation of triggered seismicity following the 1992 Landers earthquake in California. *Nature*, *406*(6795), 500–504. https://doi.org/10.1038/35020045

Ghasemizade, M., Asante, K. O., Petersen, C., Kocis, T., Dahlke, H. E., & Harter, T. (2019). An Integrated Approach Toward Sustainability via Groundwater Banking in the Southern Central Valley, California. *Water Resources Research*, *55*(4), 2742–2759. https://doi.org/10.1029/2018WR024069

Gilbert, J. M., & Maxwell, R. M. (2017). Examining regional groundwater-surface water dynamics using an integrated hydrologic model of the San Joaquin River basin. *Hydrology and Earth System Sciences*, *21*(2), 923–947. https://doi.org/10.5194/hess-21-923-2017

Goswami, J. C., & Chan, A. K. (1999). *Fundamentals of Wavelets: Theory, Algorithms, and Applications*. Wiley-Interscience.

Hanak, E., Lund, J., Arnold, B., Escriva-Bou, A., Gray, B., Green, S., Harter, T., Howitt, R., MacEwan, D., & Medellín-Azuara, J. (2017). *Water Stress and a Changing San Joaquin Valley*. Public Policy Institute of California.

Hanson, R. T., Flint, L. E., Flint, A. L., Dettinger, M. D., Faunt, C. C., Cayan, D., & Schmid, W. (2012). A method for physically based model analysis of conjunctive use in response to potential climate changes. *Water Resources Research*, *48*(2). https://doi.org/10.1029/2011WR010774

Harpold, A., Dettinger, M., & Rajagopal, S. (2017). Defining Snow Drought and Why It Matters. *Eos*. https://doi.org/10.1029/2017EO068775

Hatchett, B. J., & McEvoy, D. J. (2018). Exploring the origins of snow drought in the northern sierra nevada, california. *Earth Interactions*, *22*(2), 1–13. https://doi.org/10.1175/EI-D-17-0027.1

Healy, R. W., & Scanlon, B. R. (2010). *Estimating Groundwater Recharge*. Cambridge University Press.

Huth, A. K., Leydecker, A., Sickman, J. O., & Bales, R. C. (2004). A two-component hydrograph separation for three high-elevation catchments in the Sierra Nevada, California. *Hydrological Processes*, *18*(9), 1721–1733. https://doi.org/10.1002/hyp.1414

Jódar, J., Cabrera, J. A., Martos-Rosillo, S., Ruiz-Constán, A., González-Ramón, A., Lambán, L. J., Herrera, C., & Custodio, E. (2017). Groundwater discharge in high-mountain watersheds: A valuable resource for downstream semi-arid zones. The case of the Bérchules River in Sierra Nevada (Southern Spain). *Science of The Total Environment*, *593–594*, 760–772. https://doi.org/10.1016/j.scitotenv.2017.03.190

Johnson, C. W., Fu, Y., & Bürgmann, R. (2017). Seasonal water storage, stress modulation, and California seismicity. *Science*, *356*(6343), 1161–1164. https://doi.org/10.1126/science.aak9547

Konikow, L. F. (2015). Long-Term Groundwater Depletion in the United States. *Groundwater*, *53*(1), 2–9. https://doi.org/10.1111/gwat.12306

Lee, J. C., & Shirzaei, M. (2023). Novel algorithms for pair and pixel selection and atmospheric error correction in multitemporal InSAR. *Remote Sensing of Environment*, *286*. https://doi.org/10.1016/j.rse.2022.113447

Li, R., Ou, G., Pun, M., & Larson, L. (2018). Evaluation of Groundwater Resources in Response to Agricultural Management Scenarios in the Central Valley, California. *Journal of Water Resources Planning and Management*, *144*(12), 04018078. https://doi.org/10.1061/(asce)wr.1943-5452.0001014

Liu, F., Conklin, M. H., & Shaw, G. D. (2017). Insights into hydrologic and hydrochemical processes based on concentration-discharge and end-member mixing analyses in the mid-Merced River Basin, Sierra Nevada, California. *Water Resources Research*, *53*(1), 832–850. https://doi.org/10.1002/2016WR019437

Manning, A. H., Clark, J. F., Diaz, S. H., Rademacher, L. K., Earman, S., & Niel Plummer, L. (2012). Evolution of groundwater age in a mountain watershed over a period of thirteen years. *Journal of Hydrology*, *460–461*, 13–28. https://doi.org/10.1016/j.jhydrol.2012.06.030

Markovich, K. H., Manning, A. H., Condon, L. E., & McIntosh, J. C. (2019). Mountain-Block Recharge: A Review of Current Understanding. *Water Resources Research*, *55*(11), 8278–8304. https://doi.org/10.1029/2019WR025676

Massoud, E. C., Purdy, A. J., Miro, M. E., & Famiglietti, J. S. (2018). Projecting groundwater storage changes in California's Central Valley. *Scientific Reports*, *8*(1), 12917. https://doi.org/10.1038/s41598-018-31210-1

McCabe, G. J., Palecki, M. A., & Betancourt, J. L. (2004). Pacific and Atlantic Ocean influences on multidecadal drought frequency in the United States. *Proceedings of the National Academy of Sciences*, *101*(12), 4136–4141. https://doi.org/10.1073/pnas.0306738101

McMahon, P. B., Plummer, L. N., Böhlke, J. K., Shapiro, S. D., & Hinkle, S. R. (2011). A comparison of recharge rates in aquifers of the United States based on groundwater-age data. *Hydrogeology Journal*, *19*(4), 779–800. https://doi.org/10.1007/s10040-011-0722-5

Meixner, T., Manning, A. H., Stonestrom, D. A., Allen, D. M., Ajami, H., Blasch, K. W., Brookfield, A. E., Castro, C. L., Clark, J. F., & Gochis, D. J. (2016). Implications of projected climate change for groundwater recharge in the western United States. *Journal of Hydrology*, *534*, 124–138.

Meyer, P. L. (1970). *Introductory Probability and Statistical Applicaitons* (2nd ed.). Oxford & IBH Publishing Co.

Montgomery-Brown, E. K., Shelly, D. R., & Hsieh, P. A. (2019). Snowmelt-Triggered Earthquake Swarms at the Margin of Long Valley Caldera, California. *Geophysical Research Letters*, *46*(7), 3698–3705. https://doi.org/10.1029/2019GL082254

Mote, P. W., Li, S., Lettenmaier, D. P., Xiao, M., & Engel, R. (2018). Dramatic declines in snowpack in the western US. *Npj Climate and Atmospheric Science*, *1*(1). https://doi.org/10.1038/s41612-018-0012-1

Murray, K. D., & Lohman, R. B. (2018). Short-lived pause in Central California subsidence after heavy winter precipitation of 2017. *Science Advances*, *4*(8), eaar8144. https://doi.org/10.1126/sciadv.aar8144

Neely, W. R., Borsa, A. A., Burney, J. A., Levy, M. C., Silverii, F., & Sneed, M. (2021). Characterization of Groundwater Recharge and Flow in California's San Joaquin Valley From InSAR-Observed Surface Deformation. *Water Resources Research*, *57*(4), 1–20. https://doi.org/10.1029/2020wr028451

NOHRSC. (2004). *National Operational Hydrologic Remote Sensing Center, Snow Data Assimilation System (SNODAS) data products at NSIDC, Version 1*. National Snow and Ice Data Center, Boulder, CO, USA. https://doi.org/10.7265/N5TB14TC

Ojha, C., Shirzaei, M., Werth, S., Argus, D. F., & Farr, T. G. (2018). Sustained Groundwater Loss in California's Central Valley Exacerbated by Intense Drought Periods. *Water Resources Research*, *54*(7), 4449–4460. https://doi.org/10.1029/2017WR022250

Ojha, C., Werth, S., & Shirzaei, M. (2019). Groundwater Loss and Aquifer System Compaction in San Joaquin Valley During 2012–2015 Drought. *Journal of Geophysical Research: Solid Earth*, *124*(3), 3127–3143. https://doi.org/10.1029/2018JB016083

Pepin, N., Bradley, R. S., Diaz, H. F., Baraer, M., Caceres, E. B., Forsythe, N., Fowler, H., Greenwood, G., Hashmi, M. Z., Liu, X. D., Miller, J. R., Ning, L., Ohmura, A., Palazzi, E., Rangwala, I., Schöner, W., Severskiy, I., Shahgedanova, M., Wang, M. B., … Yang, D. Q. (2015). Elevation-dependent warming in mountain regions of the world. *Nature Climate Change*, *5*(5), 424–430. https://doi.org/10.1038/nclimate2563

Peterson, D., Smith, R., Stewart, I., Knowles, N., Soulard, C., Hager, S., & Norton, G. A. (2003). *Snowmelt Discharge Characteristics, Sierra Nevada, California.* (Series Name SIR - 2005-5056). U.S. Geological Survey.

Quiring, S. M., & Goodrich, G. B. (2008). Nature and causes of the 2002 to 2004 drought in the southwestern United States compared with the historic 1953 to 1957 drought. *Climate Research*, *36*(1), 41–52. https://doi.org/10.3354/cr00735

Rodell, M., Houser, P. R., Jambor, U., Gottschalck, J., Mitchell, K., Meng, C.-J., Arsenault, K., Cosgrove, B., Radakovich, J., Bosilovich, M., Entin*, J. K., Walker, J. P., Lohmann, D., & Toll, D. (2004). The Global Land Data Assimilation System. *Bulletin of the American Meteorological Society*, *85*(3), 381–394. https://doi.org/10.1175/BAMS-85-3-381

Saar, M. O., & Manga, M. (2003). Seismicity induced by seasonal groundwater recharge at Mt. Hood, Oregon. *Earth and Planetary Science Letters*, *214*(3–4), 605–618. https://doi.org/10.1016/S0012-821X(03)00418-7

Scanlon, B. R., Longuevergne, L., & Long, D. (2012). Ground referencing GRACE satellite estimates of groundwater storage changes in the California Central Valley, USA. *Water Resources Research*, *48*(4), W04520. https://doi.org/10.1029/2011WR011312

Schmidt, R., Flechtner, F., Meyer, U., Neumayer, K.-H., Dahle, C., König, R., & Kusche, J. (2008). Hydrological Signals Observed by the GRACE Satellites. *Surveys in Geophysics*, *29*(4–5), 319–334. https://doi.org/10.1007/s10712-008-9033-3

Schreiner-McGraw, A. P., & Ajami, H. (2022). Combined impacts of uncertainty in precipitation and air temperature on simulated mountain system recharge from an integrated hydrologic model. *Hydrology and Earth System Sciences*, *26*(4), 1145–1164. https://doi.org/10.5194/hess-26-1145-2022

Shirzaei, M. (2013). A Wavelet-Based Multitemporal DInSAR Algorithm for Monitoring Ground Surface Motion. *Ieee Geoscience and Remote Sensing Letters*, *10*(3), 456–460. https://doi.org/Doi 10.1109/Lgrs.2012.2208935

Shirzaei, M., Bürgmann, R., & Fielding, E. J. (2017). Applicability of Sentinel-1 Terrain Observation by Progressive Scans multitemporal interferometry for monitoring slow ground motions in the San Francisco Bay Area. *Geophysical Research Letters*, *44*(6), 2733–2742. https://doi.org/10.1002/2017GL072663.

Shirzaei, M., Bürgmann, R., Foster, J., Walter, T. R., & Brooks, B. A. (2013). Aseismic deformation across the Hilina fault system, Hawaii, revealed by wavelet analysis of InSAR and GPS time series. *Earth and Planetary Science Letters*, *376*, 12–19. https://doi.org/10.1016/j.epsl.2013.06.011

Shirzaei, M., Ojha, C., Werth, S., Carlson, G., & Vivoni, E. R. (2019). Comment on "Short-lived pause in Central California subsidence after heavy winter precipitation of 2017" by K. D. Murray and R. B. Lohman. *Science Advances*, *5*(eaav8038). https://doi.org/10.1126/sciadv.aav8038

Siebert, S., Burke, J., Faures, J. M., Frenken, K., Hoogeveen, J., Döll, P., & Portmann, F. T. (2010). Groundwater use for irrigation - A global inventory. *Hydrology and Earth System Sciences*, *14*(10), 1863–1880. https://doi.org/10.5194/hess-14-1863-2010

Smith, R. G., Knight, R., Chen, J., Reeves, J. A., Zebker, H. A., Farr, T., & Liu, Z. (2017). Estimating the permanent loss of groundwater storage in the southern San Joaquin Valley, California. *Water Resources Research*, *53*(3), 2133–2148. https://doi.org/10.1002/2016WR019861

Somers, L. D., & McKenzie, J. M. (2020). A review of groundwater in high mountain environments. *Wiley Interdisciplinary Reviews: Water*, *7*(6), 1–27. https://doi.org/10.1002/wat2.1475

Stevenson, S., Coats, S., Touma, D., Cole, J., Lehner, F., Fasullo, J., & Otto-Bliesner, B. (2022). Twenty-first century hydroclimate: A continually changing baseline, with more frequent extremes. *Proceedings of the National Academy of Sciences*, *119*(12). https://doi.org/10.1073/pnas.2108124119

Tague, C., & Grant, G. E. (2009). Groundwater dynamics mediate low-flow response to global warming in snow-dominated alpine regions. *Water Resources Research*, *45*(7). https://doi.org/10.1029/2008WR007179

Tague, C., Grant, G., Farrell, M., Choate, J., & Jefferson, A. (2008). Deep groundwater mediates streamflow response to climate warming in the Oregon Cascades. *Climatic Change*, *86*(1–2), 189–210. https://doi.org/10.1007/s10584-007-9294-8

Talwani, P., & Acree, S. (1985). Pore pressure diffusion and the mechanism of reservoir-induced seismicity. In *Earthquake prediction* (pp. 947–965). Springer.

Tang, Q., & Oki, T. (Eds.). (2016). *Terrestrial Water Cycle and Climate Change*. John Wiley & Sons, Inc. https://doi.org/10.1002/9781118971772

Tapley, B. D., Bettadpur, S., Ries, J. C., Thompson, P. F., & Watkins, M. M. (2004). GRACE measurements of mass variability in the Earth system. *Science*, *305*(5683), 503–505. https://doi.org/10.1126/science.1099192

Tapley, B. D., Watkins, M. M., Flechtner, F., Reigber, C., Bettadpur, S., Rodell, M., Sasgen, I., Famiglietti, J. S., Landerer, F. W., Chambers, D. P., Reager, J. T., Gardner, A. S., Save, H., Ivins, E. R., Swenson, S. C., Boening, C., Dahle, C., Wiese, D. N., Dobslaw, H., … Velicogna, I. (2019). Contributions of GRACE to understanding climate change. *Nature Climate Change*, *9*(5), 358–369. https://doi.org/10.1038/s41558-019-0456-2

Torrence, C., & Compo, G. P. (1998). A practical guide to wavelet analysis. In *Bulletin of the American Meteorological Society* (Retrieved December 5, 2018.; Vol. 79, Issue 1, pp. 61–78). https://doi.org/10.1175/1520-0477(1998)079<0061:APGTWA>2.0.CO;2

Urióstegui, S. H., Bibby, R. K., Esser, B. K., & Clark, J. F. (2017). Quantifying annual groundwater recharge and storage in the central Sierra Nevada using naturally occurring 35S. *Hydrological Processes*, *31*(6), 1382–1397. https://doi.org/10.1002/hyp.11112

USGS. (2021). *USGS Groundwater Data for the Nation*. https://waterdata.usgs.gov/nwis/gw

Vasco, D. W., Kim, K., Farr, T. G., Reager, J. T., Bekaert, D., Singh, S., & Beaudoing, H. K. (2022). Using Sentinel-1 and GRACE satellite data to monitor the long- and short-term hydrological variations within the Tulare Basin , California. *Scientific Reports*, 1–14. https://doi.org/10.1038/s41598-022-07650-1

Vrugt, J. A., Dekker, S. C., & Bouten, W. (2003). Identification of rainfall interception model parameters from measurements of throughfall and forest canopy storage. *Water Resources Research*, *39*(9). https://doi.org/10.1029/2003WR002013

Wahi, A. K., Hogan, J. F., Ekwurzel, B., Baillie, M. N., & Eastoe, C. J. (2008). Geochemical Quantification of Semiarid Mountain Recharge. *Ground Water*, *46*(3), 414–425. https://doi.org/10.1111/j.1745-6584.2007.00413.x

Wang, H. F. (2000). *Theory of Linear Poroelasticity with Applications to Geomechanics and Hydrogeology*. Princeton Univ. Press.

Welch, L. A., & Allen, D. M. (2014). Hydraulic conductivity characteristics in mountains and implications for conceptualizing bedrock groundwater flow. *Hydrogeology Journal*, *22*(5), 1003–1026. https://doi.org/10.1007/s10040-014-1121-5

Werner, C., U. Wegmüller, T. Strozzi, & A. Wiesmann. (2000). Gamma SAR and interferometric processing software. *Proceedings of the Ers-Envisat Symposium, Gothenburg, Sweden.*

White, A. M., Gardner, W. P., Borsa, A. A., Argus, D. F., & Martens, H. R. (2022). A review of GNSS/GPS in hydrogeodesy: Hydrologic loading applications and their implications for water resource research. *Water Resources Research*. https://doi.org/10.1029/2022WR032078

Yin, D., & Roderick, M. L. (2020). Inter-annual variability of the global terrestrial water cycle. *Hydrology and Earth System Sciences*, *24*(1), 381–396. https://doi.org/10.5194/hess-24-381-2020

Zektser, I. S., & Everett, L. G. (2004). *Groundwater Resources ofthe World and Their Use* (IHP-VI Series on Groundwater No. 6). United Nations Educational, Scientific and Cultural Organization (UNESCO).

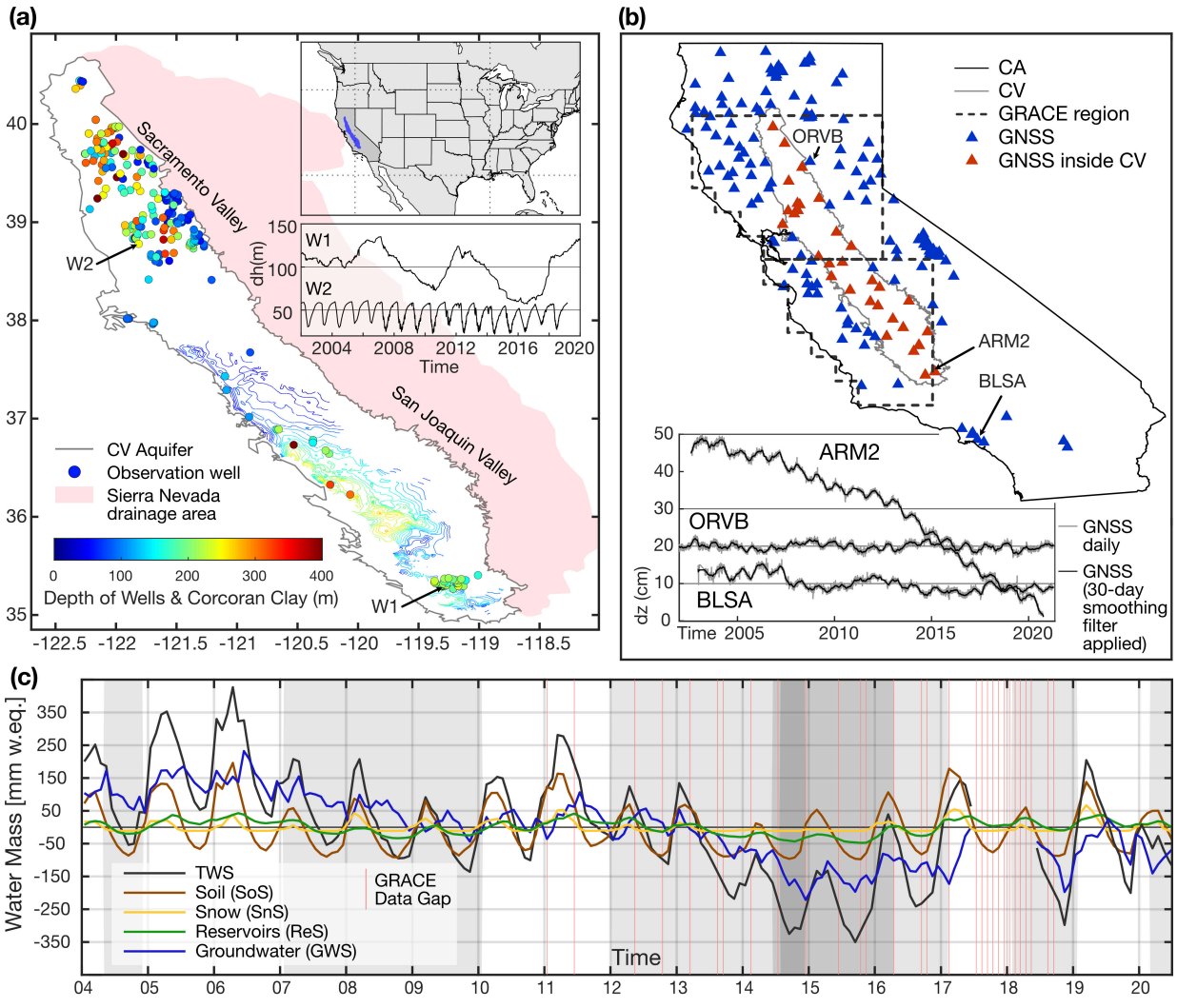

Figure 1. Overview of study area and data sets applied in this study. **(a)** Study area and hydrogeological datasets: Outline of the Central Valley aquifer system (grey line, $\boldsymbol{A_{CV}}$ = 53,672 km2), Sierra Nevada drainage area (red shade, $\boldsymbol{A_{SN}}$ = 63,780 km2), location and depth of observation wells that provide measurements at depth of 50 m and deeper, and lateral coverage and depth of the confining Corcoran clay layer (source USGS: https://water.usgs.gov/GIS/metadata/usgswrd/XML/pp1766_corcoran_clay_depth_feet.xml). See Figure S4e and S4f for histograms of well depths. Top inset indicates location of the study area over contiguous US. Bottom inset shows time series of two selected well sites W1 (#352958N1193011W001) and W2 (#387793N1218123W004). **(b)** Geodetic data sets: Mass change regions of JPL GRACE mascon solutions (black dashed line) and location of GNSS sites from the University of Reno, Nevada (red and blue triangles). Red triangles mark stations located inside the Central Valley (CV), and blue triangles those outside the CV aquifer boundary. **(c)** Time series of TWS from GRACE, composite hydrological storages and estimated GW storage are averaged for the GRACE region shown in panel a, after Ojha et al. [2019]. Gray shaded background areas (light, medium, dark gray) indicate that the USDM identifies >30% (>30%, >60%) of California's area to be in moderate (exceptional, exceptional) dry condition (compare Fig. S3).

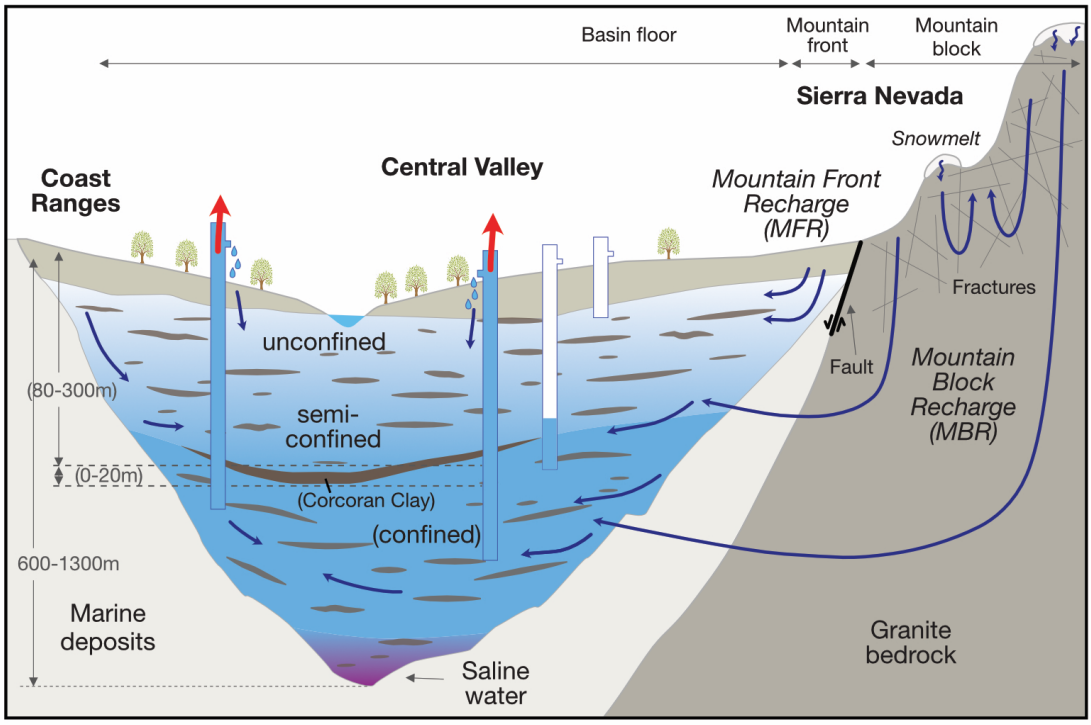

Figure 2. Conceptual and process-based model of pressure propagation and recharge in the Sierra Nevada to deep aquifer layers of the Central Valley. **(a)** Hydrogeological setting in the Central Valley (~400 m a.s.l.) and Sierra Nevada Mountains (up to ~4000 m a.s.l.). Indicated are major groundwater fluxes in and out from deep aquifer layers, including mountain front and mountain block recharge (MFR and MBR). Confining unit of the Corcoran clay is only present in the southern San Joaquin Valley, where pumping is more intense compared to the northern Sacramento Valley (Fig. 1a). This graph is inspired by Faunt et al. (2009) (Fig. A9 therein), Smith et al. (2017) (Fig. 2 therein) as well as Somers and McKenzie (2020) (Fig. 5 therein).

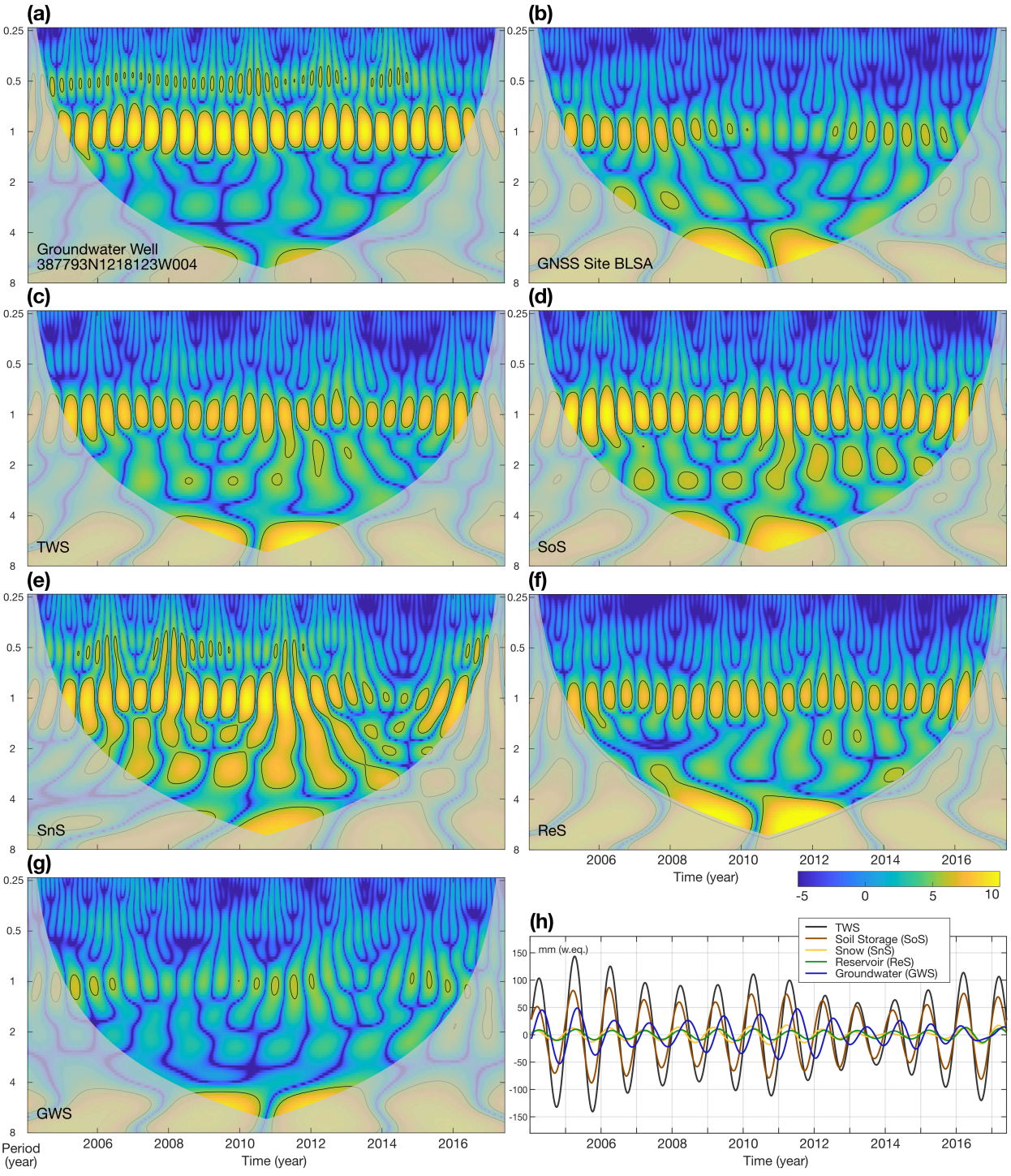

Figure 3. Wavelet time-frequency analysis. A wavelet analysis was performed for time series of all available datasets to isolate the annual signal component. Wavelet spectrum of time series of **(a)** groundwater level at well 387793N1218123W004 and **(b)** vertical land motion at GNSS site BLSA (see Fig. 1 for their location), and of average water storage variations in the GRACE region: **(c)** total water storage (TWS) from GRACE, **(d)** soil storage (SoS) from GLDAS and WGHM, **(e)** snow storage (SnS) from SNODAS, **(f)** reservoir storage (ReS) from CDWR and **(g)**

946 groundwater storage (GWS) in CV. **(h)** Reconstructed annual signal component for periods
947 within range of 0.75-0.25 years from water storage wavelet spectra shown in panel c-g.

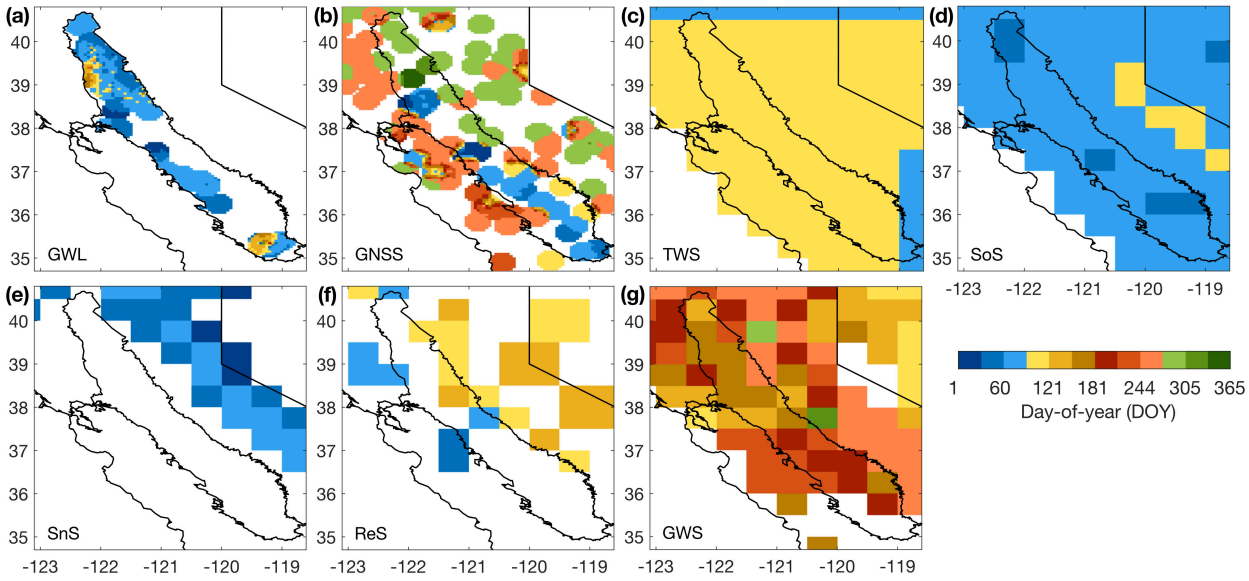

948

949 **Figure 4.** Timing of annual maximum of groundwater related signals. Timings are given in day-
950 of-year (DOY). (a) Groundwater levels (GWL) at 250 observation sites throughout the Central
951 Valley providing at least three years of data during 2002-2020 at depths below 50 m. (b) Vertical
952 land motion (maximum uplift) at 170 GNSS sites throughout entire California with a seasonal
953 amplitude larger than the median of the time series error standard deviation. Timing for
954 groundwater and GNSS were inversely interpolated using a 25 km correlation radius. Remaining
955 panels show timing of annual maximum water storage at 0.5-degree sampling resolution: (c) total
956 water storage (TWS) from GRACE, (d) soil storage (SoS) from GLDAS-Noah, (e) snow storage
957 (SnS) from SNODAS, (f) reservoir storage (ReS) from CDWR and (g) resulting groundwater
958 storage (GWS). White areas have either no data or amplitude of annual variation is near zero.
959 Annual oscillations of vertical land motion inside the CV are temporally aligned with those of
960 groundwater level variations. In contrast, oscillations of vertical land motion outside the Central
961 Valley are in resonance with annual oscillations of total water storage changes detected by
962 GRACE (compare panel b with c, and Fig. 6), because maximum VLM outside the Valley is
963 driven by minimum elastic load of the water masses. Individual values for groundwater well and
964 GNSS sites, timing of minima, related histograms, and standard deviations of annual timing
965 during observation periods are shown in Figures S8, S9, S10, and S11.

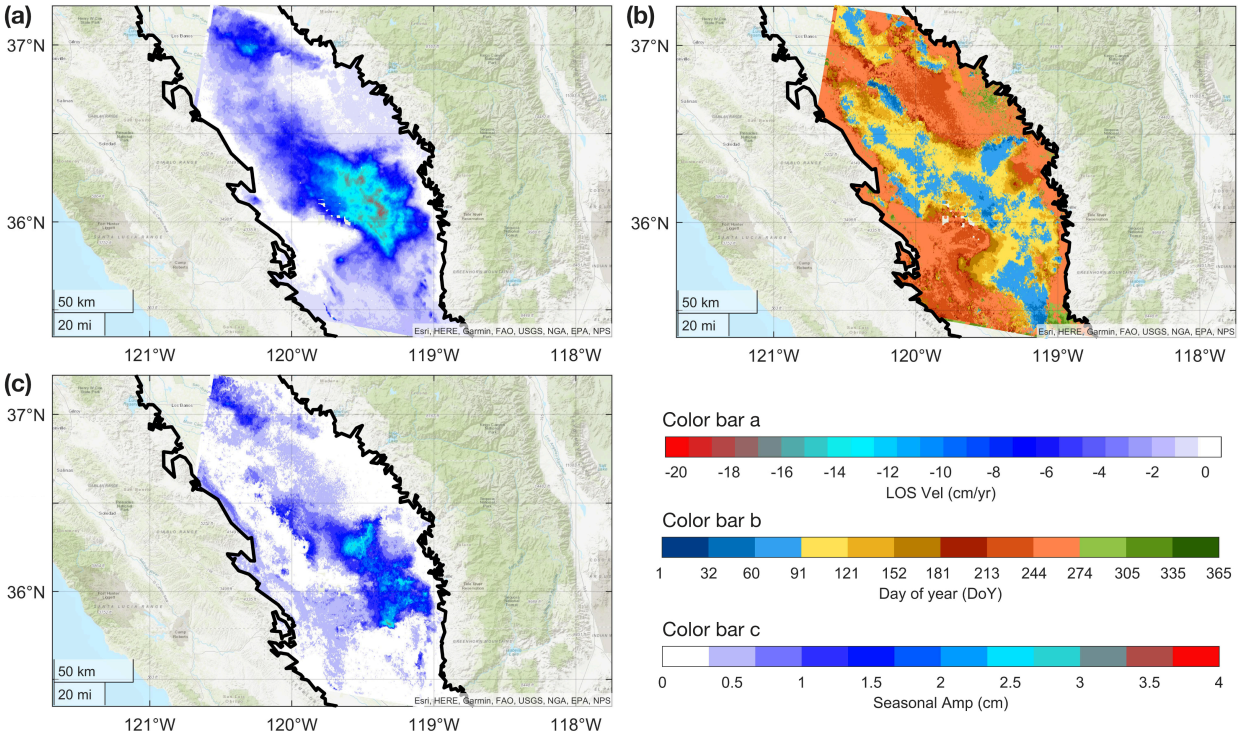

Figure 5. a) LOS velocity map for period 2015/11/27-2022/12/20. b) Median seasonal phase (peak DOY), and (c) amplitude of InSAR deformation time series for water years 2016-2022. See Figs. S15 and S16 for yearly phase and amplitude maps, respectively.

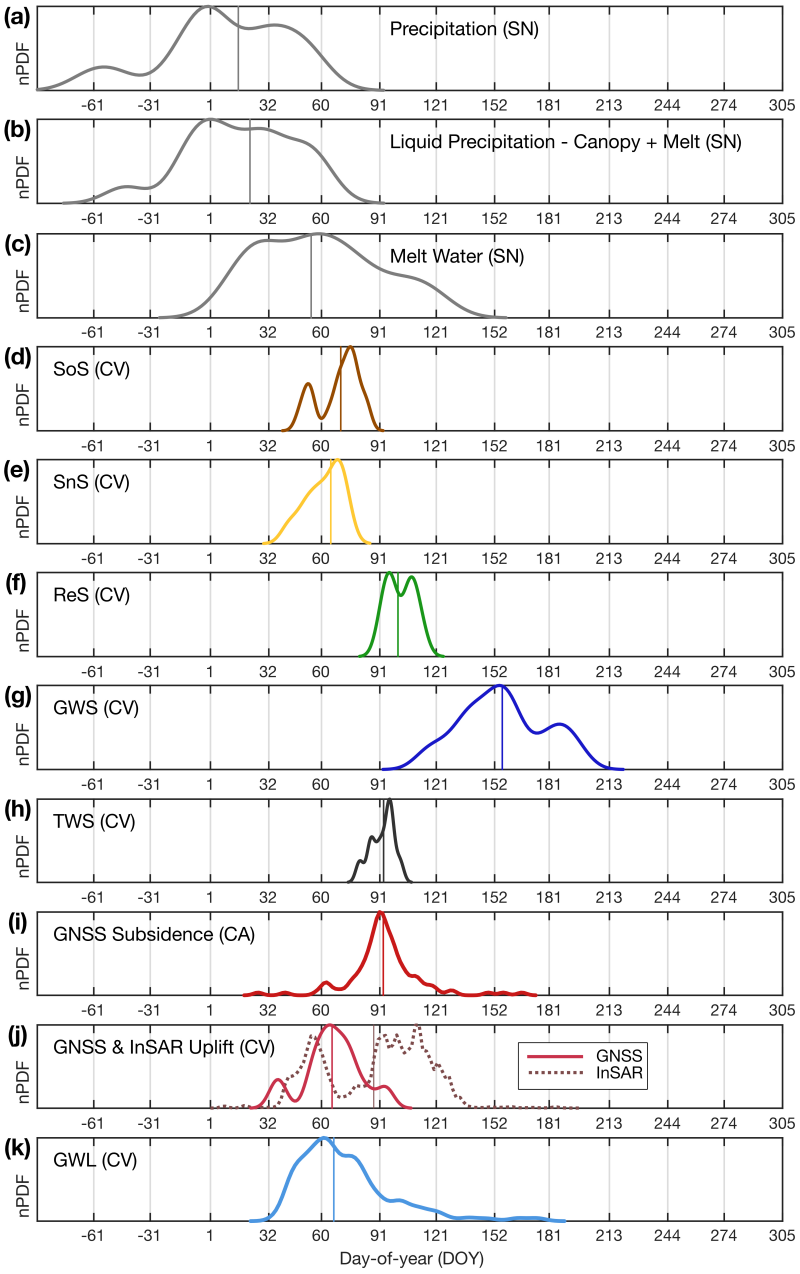

Figure 6. Normalized probability density functions for timing of annual extremes in groundwater-related signals across California. Row and line color indicate signal type: **(a)** total precipitation in the recharge area of the Sierra Nevada (SN, see Fig. 1a) from SNODAS, **(b)** Sum of liquid precipitation and melt water corrected for canopy interception in SN from SNODAS, **(c)** Melt water in SN from SNODAS, **(d)** soil storage from hydrological models for GRACE region corresponding with the Central Valley (CV, Fig. 1b), **(e)** snow storage from SNODAS for CV, **(f)** surface reservoir storage from CDWR for CV, **(g)** GRACE-based estimate of groundwater storage for CV, (H) total water storage from GRACE for CV, **(i)** vertical land motion from GNSS for all available sites in California (CA), and **(j)** for GNSS sites (red) in the CV only, and for InSAR pixels in the southern CV from Fig. 5 with a seasonal amplitude larger than 3 mm, and lastly, **(k)** groundwater levels from observation wells in CV. See Figure 1 for

location of subregions. Each function indicates maximum probability for timing of annual maximum (a-i, k) or minimum (j) amplitude of the annual signal based on wavelet analysis (Fig. 3 and Fig. S7). Vertical lines represent the mean value for timing of annual maximum. Distribution is normalized by maximum probability density value and results from year-to-year variation of the regionally averaged gridded datasets (a-h) and from spatial variation of well and GNSS data sets (i-k).

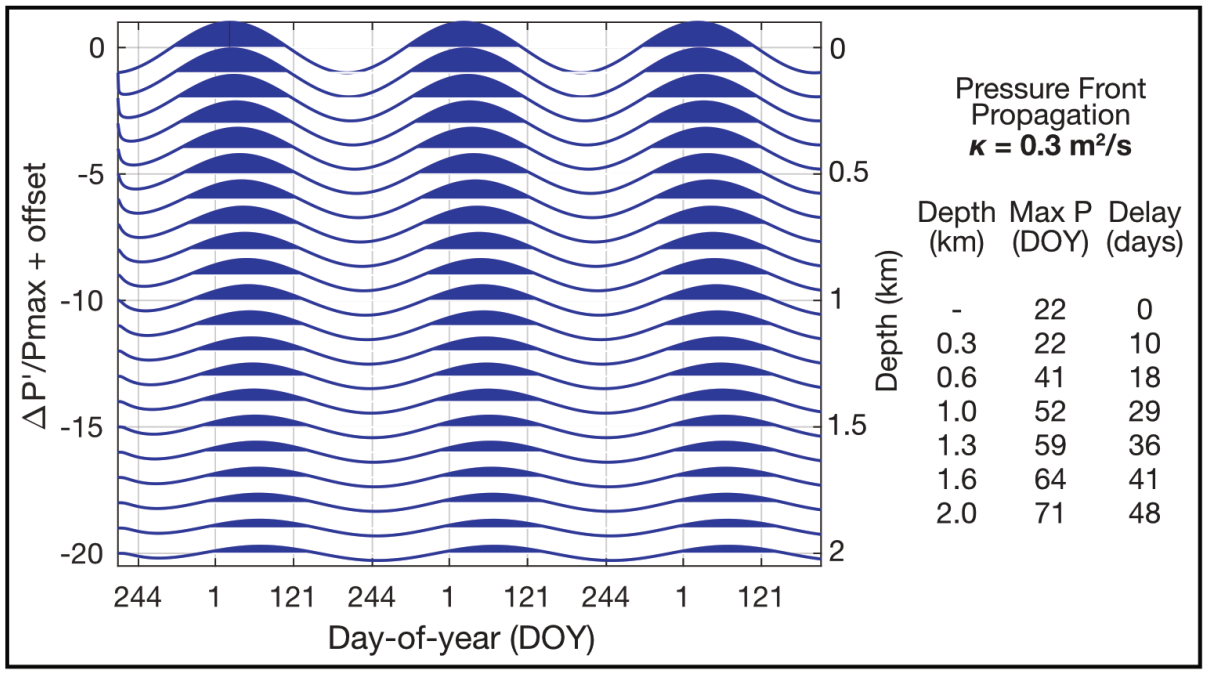

Figure 7. Vertical pressure propagation for elevation difference between the Sierra Nevada Mountains and the Central Valley aquifers. Normalized pressure change ($\Delta P'/P_{max}$) at different depth due to standard 1D calculation of pressure front propagation along mountain block recharge conduits in the fractured bedrock of the Sierra Nevada Mountains. Graphs are incrementally offset by -1 for each depth. In top groundwater layers, maximum pressure occurs on January 22nd (DOY 22), which is driven by mean annual water availability in the recharge area (Fig. 6b). Table to the right indicates DOY and time delay of the pressure propagation to depth of 300-2000 m. Given a hydraulic diffusivity κ = 0.3 m^2/s (reasonable for fractured granite bedrocks), the pressure front needs ~0.6 (1.2, 1.6) months to propagate to depth of 600 (1300, 2000) m. A smaller hydraulic diffusivity would lead to a slower propagation to depth and vice versa, examples for κ = 0.5, 0.1 m^2/s are shown in Figure S14.